Available online at www.sciencedirect.com
ScienceDirect
Journal of the European Ceramic Society 27 (2007) 2163–2169
www.elsevier.com/locate/jeurceramsoc

Thermal expansion study of spinel-sialon

T. Gross [a,*], M. Schwarz [b], M. Knapp [a,c], E. Kroke [b], H. Fuess [a]

[a] *Institute for Materials Science, Darmstadt University of Technology, Petersenstr. 23, D-64287 Darmstadt, Germany*
[b] *Department of Chemistry, University of Technology Bergakademie Freiberg, Leipziger Str. 29, D-09596 Freiberg, Germany*

Received 7 October 2005; received in revised form 8 July 2006; accepted 15 July 2006
Available online 12 September 2006

Abstract

The thermal expansion behaviour of a high pressure-derived spinel sialon (γ-$Si_{3-x}Al_xO_xN_{4-x}$) with a single composition $x = 1.1$ (and its low-pressure pendant with β-Si_3N_4 structure) was studied between room temperature and 1220 °C, using X-ray diffraction at a synchrotron radiation source and a halogen mirror furnace. No evidence for a phase transformation or decomposition of the spinel-sialon was found, thus demonstrating a good metastability of this novel hard material.
© 2006 Elsevier Ltd. All rights reserved.

Keywords: Thermal expansion; Sialon; Spinel-sialon; Si_3N_4

1. Introduction

After the discovery of the high pressure phase of Si_3N_4 with spinel structure (γ-Si_3N_4) in 1999 by Zerr et al.,[1] it was shown that a solid solution series of spinel-sialon (γ-$Si_{3-x}Al_xO_xN_{4-x}$), in analogy to the well-known phase relationship β-Si_3N_4 ⋯ β-$Si_{3-x}Al_xO_xN_{4-x}$[d] (beta-sialons)[3,4] exists. The stability field of β-sialon is known to be $0 < x < 2.1$ for $Si_{3-x}Al_xO_xN_{4-x}$.[5–7] In this system the Si-atoms are substituted by Al-atoms and N- by O-atoms, respectively. Extensive studies of the system (M)–Si–Al–O–N (or α-sialons with (M) being a metal cation such as Li, Ca, Y and many of the rare earth ions) and the more fundamental system Si–Al–O–N (e.g. β-sialons) as well as other sialons have already been performed since the 1970s by Jack et al.[8,9] and numerous reviews are available on the subject [10,2,11,12]. No corresponding measurements of the material properties of spinel-$Si_{3-x}Al_xO_xN_{4-x}$ (with $0 \le x \le 2.1$) have been reported yet. The reasons are the novelty of the material as well as its extreme synthesis conditions. Most of the available literature on this material is of theoretical nature. These reports predict a large direct bandgap, which is proposed to be adjustable with the degree of substitution x.[13–15] Furthermore, the high postulated hardness of γ-Si_3N_4 just as well as γ-$Si_{3-x}Al_xO_xN_{4-x}$ [13,14] has been experimentally proven.[16–18,4] Their hardness values measured so far (35 GPa for γ-Si_3N_4 [18,16] and 28 GPa HV_1 for γ-Si_2AlON_3 [4]) qualify these materials as good candidates for cutting or abrasive applications. The thermal stability for γ-Si_3N_4 to 1400 °C in air has been demonstrated,[16,19] thus emphasizing its potential application as high temperature material under oxidising conditions. Precise knowledge about the thermomechanical properties is fundamental for this material class. γ-Si_3N_4 shows a linear thermal expansion coefficient of $\alpha = 3\text{–}4 \times 10^{-6}\,K^{-1}$ at room temperature which increases above $\sim 6 \times 10^{-6}\,K^{-1}$ at 1000 °C,[17,20] thus being two to three times larger than that of β-Si_3N_4 ($\alpha \approx 1\text{–}3 \times 10^{-6}\,K^{-1}$),[21] but comparable to the III–V nitrides such as GaN[22] or hard nitrides like TiN and ZrN. For "doped" γ-Si_3N_4, respectively, γ-$Si_{3-x}Al_xO_xN_{4-x}$, the thermal expansion coefficients have not been reported yet in literature.

2. Sample preparation

The synthesis of the β-sialon has been described in our previous report.[4] The degree of substitution x in the β-sialon was checked by the known dependence of unit cell parameters,[7] electron probe microanalysis (EPMA, Si:Al-ratio) and combustion elemental analysis (O and N content). According to these measurements, x lies between 1.07 and 1.12 as an upper and lower bound.[23] The grain sizes of the starting β-sialon sample ranged

* Corresponding author. Tel.: +49 6151 16 6359; fax: +49 6151 16 6023.
E-mail address: gross@st.tu-darmstadt.de (T. Gross).
[c] Current address: CELLS, P.O. Box 68, 08193 Barcelona, Spain.
[d] For β-sialon, often the formula $Si_{6-z}Al_zO_zN_{8-z}$ is used. Here we follow the recommendation of Ekström and Nygren [2] that indicates the Si_3N_4 parent phase more clearly. Moreover, a better resemblance to the general formula for spinel-compounds AB_2X_4 is achieved.

0955-2219/$ – see front matter © 2006 Elsevier Ltd. All rights reserved.
doi:10.1016/j.jeurceramsoc.2006.07.007

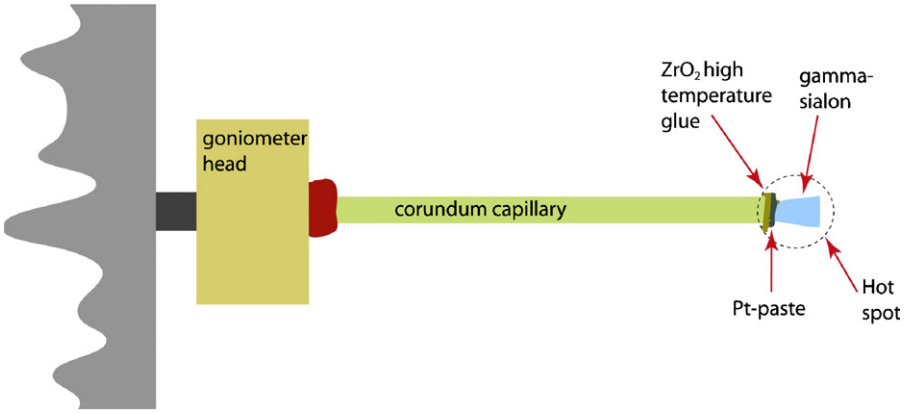

Fig. 1. Schematic picture of the assembly. The parts of the assembly from left to right: rotatable sample holder, goniometer head, corundum capillary, zirconia (high temperature) glue, Pt paste and gamma-sialon.

between 0.9 and 2.5 μm as determined by SEM. In our previous study it has also been shown, that the transition to the high pressure phase does not affect the composition (i.e. degree of substitution x) of the material. The recovered sample after the high temperature/high pressure (HT/HP)-synthesis is a polycrystalline solid. Grinding of the obtained material to a powder is not recommended, as other measurements (indentation hardness testing, SEM, TEM, etc.) can better be done on a solid body sample than in powder form.

For the measurements of β-sialon, thin, free standing bars ~0.2 mm thick and 5 mm in length were cut from the hot-pressed polycrystalline body using a diamond wire saw.

The recovered high-pressure spinel-sialon sample is an opaque polycrystalline solid with grain sizes ≤ 1 μm. Similar to the β-sialon it was cut into a bar-shaped body directly out of the surrounding ceramic high pressure cell. Adhering remains of the encapsulation materials (i.e. MgO, $LaCrO_3$) and their reaction products with the spinel-sialon were removed via successive embedding and grinding steps.

The sample itself was glued on a corundum capillary (see Fig. 1), using a high temperature glue (904 zirconia ultrahigh-temp adhesive, Cotronics Corp., Brooklyn, NY, USA). The X-ray beam was incident perpendicular to the axis of the capillary/sample and collimated to a broad cross-section of ≃2 mm × 2 mm, thus covering the sialon-bar and the Pt-coated part of the corundum capillary with the ZrO_2-glue. In some of the consecutive measurements, the sample was aligned so that the beam did not hit the Al_2O_3 capillary (see Section 5).

In order to provide a temperature standard, the corundum capillary was treated with a Pt-paste (Pt-paste; Chempur® platinum conducting paste 71% Pt) on its outer edge. *Direct* contact between sample and Pt-paste was to be avoided, as in previous HP/HT synthesis experiments, formation of Pt–silicides at the interface between sialon and the Pt metal, used for sample encapsulation had been observed. Pt is commonly used as temperature standard in (high temperature) diffraction, because it gives sharp reflections up to its melting point (T_m ~ 1770 °C) and is not affected by oxidising environments. The dependency between its lattice parameter and T is well described in literature.[24,25] The residues of the solvent of the Pt-paste were eliminated by heating the sample in the furnace above 1000 °C before measuring.

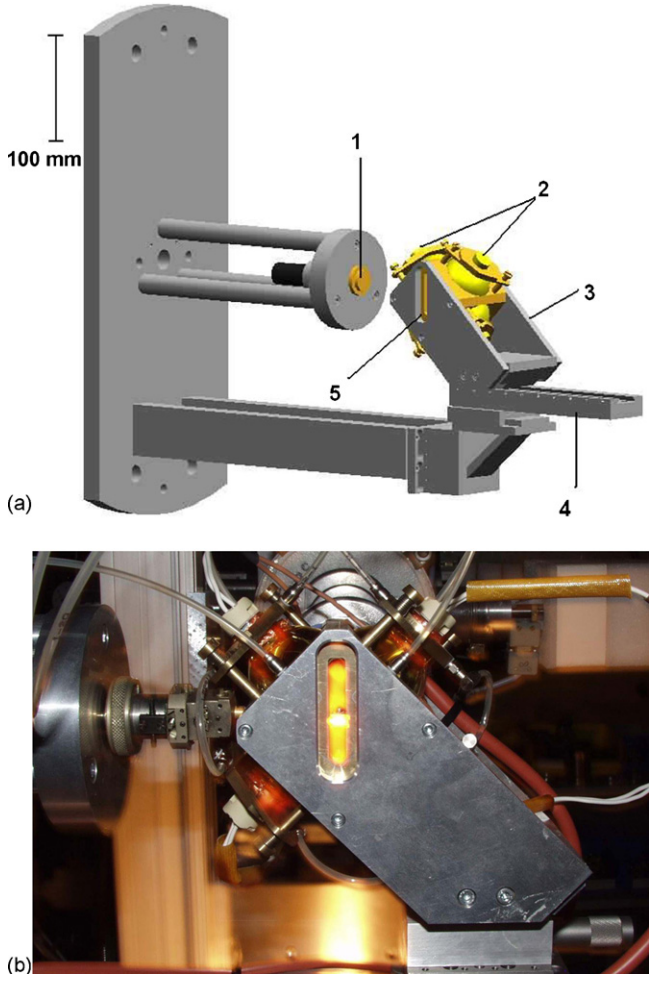

Fig. 2. (a) A schematic drawing of the furnace: (1) (rotatable) sample holder, (2) halogen lamp, (3) (water-cooled) furnace hull, (4) guide rail to move the furnace into and out of the beam, and (5) exit slit. (b) Photography of the furnace.

3. Temperature measurement

The halogen mirror furnace[26] operates under normal atmospheric (i.e. oxidising) conditions. The measurement assembly is shown in Figs. 1 and 2. Four halogen lamps, with a DC power supply and a maximum power output of 4 × 150 W, are focussed

in a single spot—the hot spot of the furnace (∼ 0.5 mm^2). Power control was accomplished by a type B thermocouple located opposite to the sample and being connected to a feedback loop system (Eurotherm® 2404). The capillary with the sample was fixed on a goniometer head in order to improve counting statistics during the measurement via sample rotation.

The thermocouple (TC) was placed at a distance of ∼2–3 mm from the sample, that itself was centered in the hot spot, in order to prevent (i) mechanical damage, (ii) chemical reactions and (iii) further reflections in the XRD pattern that may have overlapped with those of the sialon.

In order to account for the thermal asymmetry between the locus of the sample and the TC, and to avoid a temperature overshoot, which eventually might have led to decomposition of the high pressure γ-sialon sample, the more readily available β-sialon bars with the same composition (i.e. with $x = 1.1$) and approximate dimensions as the γ-sialon were measured first. With the synchrotron beam hitting both, the sample and the Pt-coated alumina (along with the zirconia high temperature glue), this provided a power calibration for the later measurements. The heating device was set to a distinct temperature reading of the TC. When it was equilibrated, both power and heating current were recorded. After the evaluation of the diffraction pattern, the lattice parameters of Pt were used to determine the real sample temperature. In that manner, a rough correlation between the temperature in the hot spot and the total heating power was established. As a result, the temperature reading from the TC showed much lower values for the temperatures than the ones obtained from the lattice parameters of Pt. In the high temperature regime of the measurement the maximum difference was 450 °C, which is not surprising as the hot spot is very small and thermal radiation decays rapidly with distance.

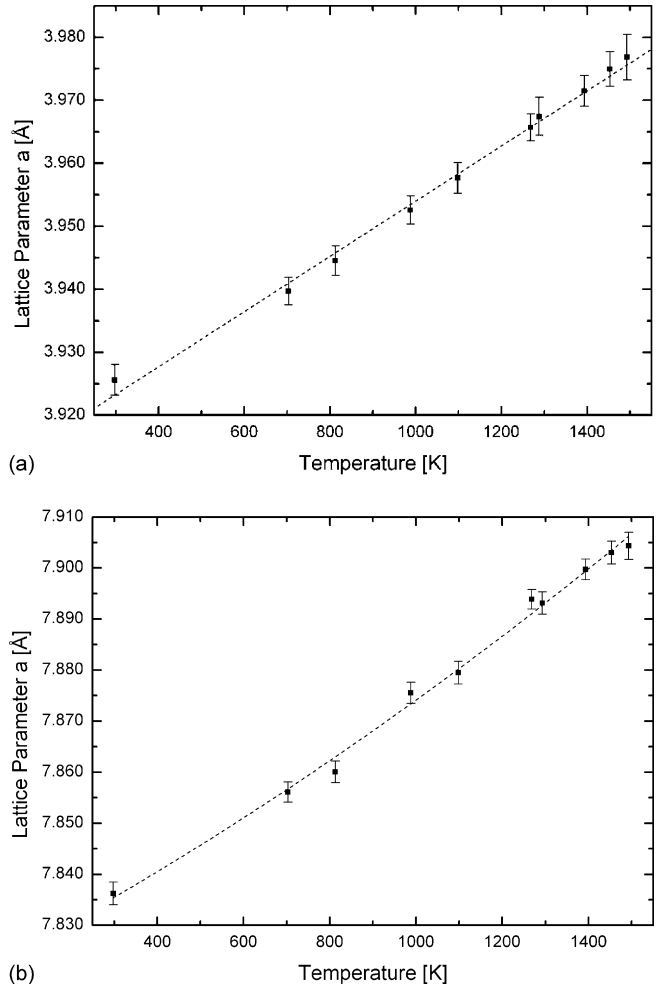

Fig. 3. Lattice parameter a of Pt (internal temperature standard) (a) and γ-sialon (b) vs. temperature; the according fitting curve of the obtained data is also displayed.

For a simple metal with a *fcc* structure like Pt and with the help of the Rietveld method, it is sufficient to use a couple of reflections to determine lattice parameter very accurately. In this case, the first five reflections of Pt were used to determine its lattice parameters as a function of T. The error bars in Fig. 3(a) and (b) as well as the values given in parentheses in Tables 1 and 2 represent the statistical standard deviations ("correlated residuals"),[27] as obtained from the structure refinements. The obtained lattice parameters for Pt are adequately precise for the determination of the temperature, whereas the polynomials describing this dependency (see Eqs. (2)–(4)) exhibit an uncertainty on the temperature. On that behalf the temperatures that were obtained in this manner, were rounded off in 5 °C steps.

4. Data acquisition

Diffraction data were collected at beamline B2 at HASYLAB/DESY (Hamburg Synchrotronstrahlungslabor/Deutsches Elektronen Synchrotron).[28] A full pattern and selected regions were measured with a single scintillation counter using parallel foils ("soller slits") as optical element in front of the detector to define the resolution. The setup was optimized for maximum intensity along with sufficient resolution and short acquisition time. The instrumental resolution with this setup was ∼0.1° (2θ).

The full pattern was recorded at room temperature. Because the angular detection range is limited by the opening angle of the exit slit of the furnace (∼38° (2θ), relative to the primary beam), a wavelength of $\lambda = 0.695217$ Å was selected, resulting in a measurement range of 8–37.3 ° (2θ) which covered the first 16 reflections of the spinel-sialon.

After analysing the full pattern (see Fig. 4), it was decided not to measure the whole range, but to leave out certain angular ranges where no reflections occur. To save measuring time at elevated temperatures, only selected ranges were measured.[e] The acquisition time for the selected ranges at each temperature (temperature sequence: 430 °C, 715 °C, 995 °C, 1120 °C, 1180 °C, 1220 °C, 1015 °C, 825 °C and 540 °C[f]) was 90–120 min, depending on the actual synchrotron beam current. Before data acquisition the sample was given about 15 min to reach thermal equilibrium.

[e] The selected angular ranges were: 8–9°, 11–23.25° and 25–37.3° (2θ).

[f] The temperatures that are given here are already the temperatures according to the refined unit cell parameter of the internal temperature standard (Pt) according to.[29]

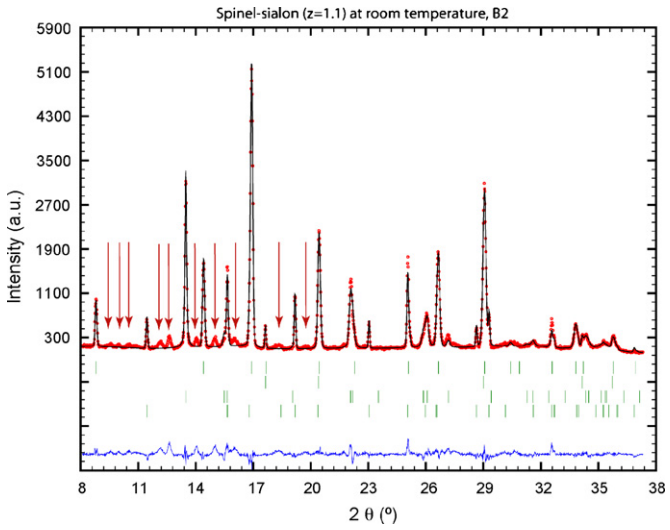

Fig. 4. Full pattern at room temperature; the phases are from top to bottom: γ-$Si_{3-x}Al_xO_xN_{4-x}$ (with $x = 1.1$), Pt (internal temperature standard), α-corundum capillary (sample holder), tetragonal ZrO_2 (high temperature glue). The arrows point to some not indexed reflections; most of them could be assigned to monoclinic ZrO_2, which originates from the high temperature glue. Because of the low phase content, the monoclinic phase was not taken into account until its phase content grew considerably. Obviously some of the tetragonal ZrO_2 transformed into monoclinic ZrO_2 (or the latter experienced grain growth) after being heated for several hours. However, growing amount of the monoclinic ZrO_2 could not be detected until heating above 1200 °C and then slowly cooling down. As the temperature dropped to 825 °C, the conversion tetragonal ⇒ monoclinic can clearly be observed, therefore the monoclinic phase could not be neglected anymore. Therefore, it was also taken into account for the last two collected patterns (∼825 °C and ∼540 °C). The difference plot is also displayed.

5. Results and discussion

Full pattern analysis was done via the Rietveld method with the WINPLOTR software package.[30] Six structural models were used to describe the data adequately: β-sialon, γ-sialon, α-corundum (sample holder), Pt (internal temperature standard) and tetragonal/monoclinic ZrO_2 (high temperature glue). During the entire heat treatment with a peak temperature of 1220 °C for 90 min, no indications for a phase-transformation or decomposition of the gamma-sialon were found, thus demonstrating a considerable metastability of this hard high pressure-derived material. Further investigation on the possible oxidation of the sialon surface is under way.

The lattice parameters of the β-sialon, the internal temperature standard (Pt) and the γ-sialon, respectively, that have been obtained from Rietveld-refinement, have been combined in Tables 1 and 2 along with the calculated standard deviations (in parentheses; they also represent the error bars in Fig. 3). For better comparison the values of the lattice parameters of β-sialon have been normalised to their value at room temperature (see Fig. 5). For the beta-sialon measurements the sample was prepared and aligned so good, that the collected patterns did not show the reflections of the corundum capillary at all. Thus, all reflections can clearly be attributed to the phases used in the structural models (furthermore the reflection positions of the hexagonal beta-sialon are not overlapping with the temperature standard Pt).

Table 1
Lattice parameters of β-sialon and Pt obtained from Rietveld-refinement

Temperature (°C)	a(β) (Å)	c(β) (Å)	a(Pt) (Å)
28	7.667 (8)	2.963 (4)	3.924 (7)
220	7.672 (7)	2.965 (3)	3.931 (8)
275	7.673 (7)	2.966 (3)	3.934 (7)
350	7.676 (8)	2.967 (3)	3.937 (8)
430	7.678 (8)	2.968 (3)	3.941 (8)
500	7.682 (9)	2.970 (4)	3.946 (10)
575	7.686 (9)	2.971 (4)	3.951 (10)
635	7.689 (11)	2.973 (5)	3.956 (12)
700	7.692 (12)	2.974 (5)	3.962 (13)

The estimated standard deviations (in parentheses) are calculated according to.[33]

Table 2
Lattice parameters of γ-sialon and Pt obtained from Rietveld-refinement

Temperature (°C)	a(γ) (Å)	a(Pt) (Å)
28	7.836 (2)	3.926 (2)
430	7.856 (2)	3.940 (2)
540	7.866 (2)	3.945 (2)
715	7.876 (2)	3.953 (2)
825	7.879 (2)	3.958 (2)
995	7.894 (2)	3.966 (2)
1015	7.893 (2)	3.967 (3)
1120	7.900 (2)	3.972 (2)
1180	7.903 (2)	3.975 (3)
1220	7.904 (3)	3.977 (4)

As the gamma-sialon sample was considerably smaller, it was not possible to prepare and mount the sample as good as the beta-sialon (i.e. without measuring the corundum capillary). Nevertheless all of the reflections could be explicitly related to their originating phases, although some of them are strongly overlapping in the diffractogram at room temperature. Because of peak shifts due to different thermal expansion, some overlapping reflections separated at elevated temperatures. Furthermore, the gamma-sialon and the Pt phases both show non-overlapping

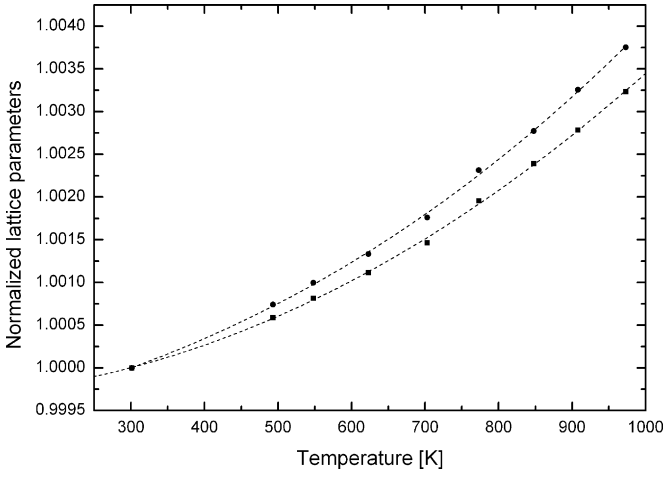

Fig. 5. Normalized (to the value for room temperature) lattice parameters a and c of β-sialon, respectively. The solid squares represent data of the lattice parameter a (■) and the solid circles those of lattice parameter c (●). Fitted curves of both data sets are also displayed as guide to the eye.

reflections at room temperature ((1 1 1) and (2 2 0) for gamma-sialon and (1 1 1) for Pt). The resulting reflection positions were therefore sufficient for the determination of the lattice constants.

Temperatures have been approximated numerically by the usage of the Pt unit cell parameter with the help of Eq. (1) according to[29] (with the coefficients a_1–a_4 stated there):

$$a(T) = \sum_{\nu=1}^{N} a_\nu T^{(\nu-1)} = a_1 + a_2 T + a_3 T^2 + a_4 T^3 + \cdots \quad (1)$$

The obtained data (i.e. lattice constants as function of the temperature) can be fitted to a polynomial function in a similar form to the one for Pt as stated above

$$a_\beta(T)\,(\text{Å}) = 7.665 + 2.854 \times 10^{-8} T^2 + 4.400 \times 10^{-13} T^3 \quad (2)$$

$$c_\beta(T)\,(\text{Å}) = 2.962 + 1.417 \times 10^{-8} T^2 - 1.178 \times 10^{-12} T^3 \quad (3)$$

$$a_\gamma(T)\,(\text{Å}) = 7.821 + 4.0 \times 10^{-5} T + 8.307 \times 10^{-9} T^2 - 5.0 \times 10^{-5} \frac{1}{T} \quad (4)$$

However, the obtained data for γ-sialon did not comply to a third order polynomial fit, hence another fitting routine of the data was chosen. It was described before by Paszkowicz et al.[20] and was used for the high temperature branch of their measurements. It is a second order polynomial function with an additional $(1/T)$ term (see Eq. (4)). With the established Eqs. (2)–(4) (i.e. lattice parameters versus temperature), the linear thermal expansion coefficient was calculated according to its definition[g]:

$$\alpha(T) = \frac{1}{f(T)} \frac{\partial f(T)}{\partial T} \quad (5)$$

For β-sialon it is displayed temperature-dependant in Fig. 6 in both possible crystallographic directions (for the investigated temperature region). A slight anisotropy of thermal expansion coefficients in those directions can clearly be seen in Fig. 6. For better comparison both figures were scaled equally. The values of the linear thermal expansion are $(2.25\text{–}7.4)\times10^{-6}\,\text{K}^{-1}$ for the a-parameter and $(2.7\text{–}8.15)\times10^{-6}\,\text{K}^{-1}$ for the c-parameter in the observed temperature region. These values are in good agreement with those reported in literature, which are $(2\text{–}4)\times10^{-6}\,\text{K}^{-1}$ depending on the degree of substitution z and the temperature.[31]

Fig. 7 displays the different atomic distances (versus temperature) as obtained from the refinements of the structure along with their calculated standard deviations (represented by the error bars). Fig. 7(a) shows the (Si,Al)–(O,N) distances: the upper curve (black squares) represents the distances for octahedral coordinated anions [16d site] whereas the lower curve (closed black circles) represents the distances for tetrahedral coordinated anions [8a site]. Fig. 7(b) displays the atomic distances for

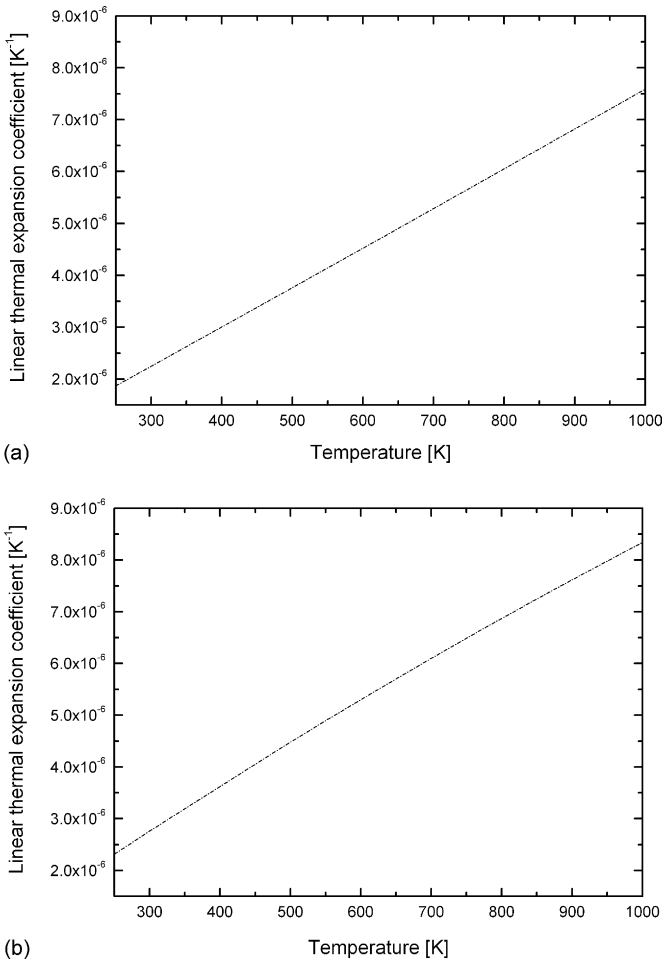

Fig. 6. Linear thermal expansion coefficient for β-sialon (a) in a-direction and (b) c-direction, respectively, vs. temperature.

(Si,Al)–(Si,Al) (upper curve; black squares) and (O,N)–(O,N) (lower curve; closed black circles).[h] The only clear trend (strictly monotonic increasing) can be made out for distances of octahedral coordinated (Si,Al)–(O,N) [16d site], which is not surprising as it is directly correlated to the expanding structure, due to the rising temperature.

The resulting function for γ-sialon is displayed in Fig. 8. As there are no measurements available for γ-sialon, the values will be compared to γ-Si_3N_4 as one end member in the solid solution series. The available literature clearly reveals a pronounced dependency of the value of alpha from the used fitted polynomial function $\alpha(T)$.

Jiang et al.[17] report $(4\text{–}6.5)\times10^{-6}\,\text{K}^{-1}$ in the temperature range 26.85–726.85 °C, whereas Hintzen et al.[32] report $(3\text{–}8)\times10^{-6}\,\text{K}^{-1}$ for the same temperature region and $(4\text{–}6.5)\times10^{-6}\,\text{K}^{-1}$ for γ-Si_3N_4. Usage of Eq. (4) gives the values $(5.7\text{–}8.2)\times10^{-6}\,\text{K}^{-1}$ for the γ-sialon ($x = 1.1$) in the observed temperature region (26.85–1226.85 °C) which seems reasonable

[g] In which $f(T)$ represents one of Eqs. (2)–(4).

[h] The curves (dotted lines) are just depicted as guide to the eye. They do not represent the 'real' physical behaviour. Unfortunately, the obtained data is not sufficiently accurate to make reliable statements about the further progression of the atomic distances.

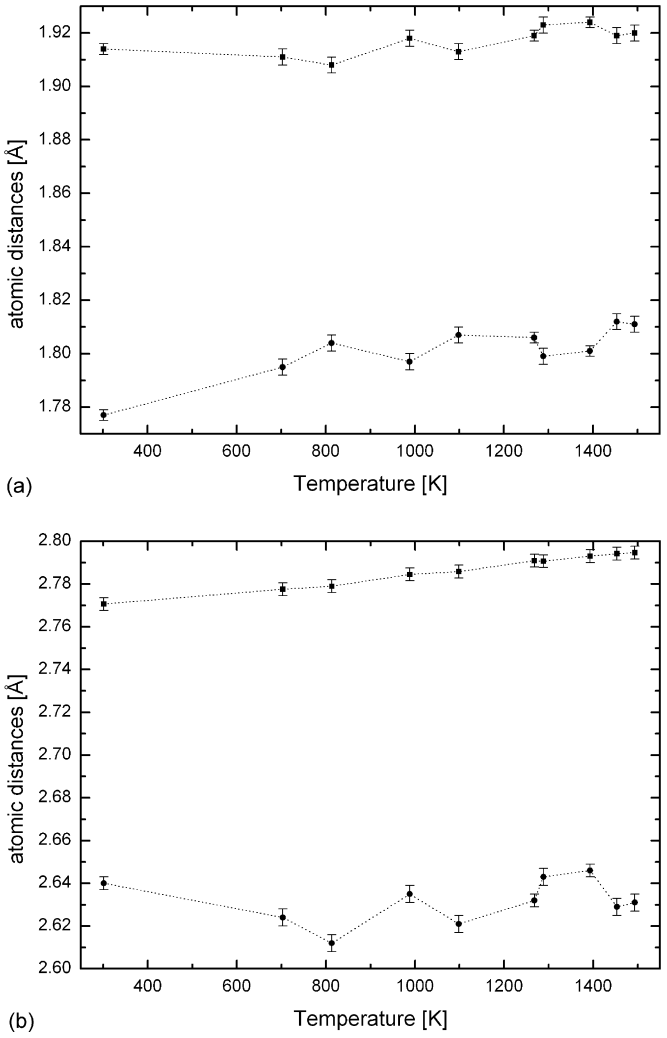

Fig. 7. Atomic distances for γ-sialon obtained from structure refinement. (a) (Si,Al)–(O,N) distances: black squares represent the distances for octahedral coordinated anions [16d site], closed black circles the distances for tetrahedral coordinated anions [8a site]. (b) Black squares depict (Si,Al)–(Si,Al) distances, (O,N)–(O,N) closed black circles distances.

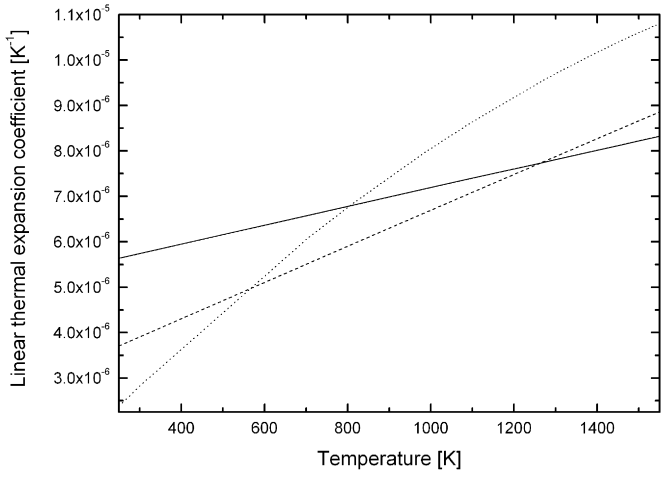

Fig. 8. Linear thermal expansion coefficient for γ-sialon vs. temperature (solid line) along with the data for γ-Si_3N_4 obtained by Jiang et al.[17] (dashed line) and Hintzen et al.[32] (dotted line). The other data were extrapolated to higher temperatures than 726.85 °C for better comparison.

compared to the parent phase. As the cubic Si_3N_4 is more covalent than γ-sialon it can be expected that the thermal expansion coefficients of the latter should be a little bit larger, which is the case.

Acknowledgments

The financial support of this work by the *Deutsche Forschungsgemeinschaft; Project Nos. KR 1739/8-1 and FU 125/39* is gratefully acknowledged. We also thank *Bayerisches Geoinstitut* for technical and advisory support with the multi-anvil press experiments, especially Dan Frost and the people of the excellent workshop there. A special thanks goes to Paul Erhart for fruitful discussions and help with some numerical models.

References

1. Zerr, A., Miehe, G., Serghiou, G., Schwarz, M., Kroke, E., Riedel, R., et al., Synthesis of cubic silicon nitride. *Nature*, 1999, **400**(6742), 340–342.
2. Ekström, T. and Nygren, M., SiAlON ceramics. *J. Am. Ceram. Soc.*, 1992, **75**(2), 259–276.
3. Sekine, T., He, H., Kobayahi, T., Tansho, M. and Kimoto, K., Cubic $Si_{6-z}Al_zO_zN_{8-z}$ ($z = 1.8$ and 2.8) spinels formed by shock compression. *Chem. Phys. Lett.*, 2001, **344**(3/4), 395–399.
4. Schwarz, M., Zerr, A., Kroke, E., Miehe, G., Chen, I. -W., Heck, M. et al., Spinel sialons. *Angew. Chem. Int. Ed.*, 2002, **41**(5), 789–793.
5. Gauckler, L. J., Lukas, H. L. and Petzow, G., Contribution to the phase diagram Si_3N_4–AlN–Al_2O_3–SiO_2. *J. Am. Ceram. Soc.*, 1975, **58**(7/8), 346–347.
6. Jack, K. H., The significance and structure and phase equilibria in the development of silicon nitride and sialon ceramics. *Sci. Ceram.*, 1981, **11**, 125–142.
7. Ekström, T., Käll, P. O., Nygren, M. and Olsson, P. O., Dense single-phase beta-sialon ceramics by glass-encapsulated hot isostatic pressing. *J. Mater. Sci.*, 1989, **24**(5), 1853–1861.
8. Jack, K. H. and Wilson, W. I., Ceramics based on silicon nitride. *Nature*, 1972, **238**(5360), 128–129.
9. Oyama, Y. and Kamagaito, O., Solid solubility of some oxides in Si_3N_4. *Jpn. J. Appl. Phys.*, 1971, **10**(11), 1342–1637.
10. Mitomo, M., Sialon ceramics. *Kagaku Kogyo*, 1985, **36**(1), 31–34.
11. Izhevskiy, V. A., Genova, L. A., Bressiani, J. C. and Aldinger, F., Progress in SiAlON ceramics. *J. Eur. Ceram. Soc.*, 2000, **20**(13), 2275–2295.
12. Raju, C. B., Verma, S., Sahu, M. N., Jain, P. K. and Choudary, S., Silicon nitride/SiAlON ceramics—a review. *Indian J. Eng. Mater. Sci.*, 2001, **8**(1), 36–45.
13. Ouyang, L. and Ching, W. Y., Structure and bonding in a cubic phase of SiAlON derived from the cubic spinel phase of Si_3N_4. *Appl. Phys. Lett.* 2002, **81**(2):229–231.
14. Lowther, J. E., Schwarz, M., Kroke, E., Riedel, R., Electronic structure calculation of cohesive properties of some $Si_{6-z}Al_zO_zN_{8-z}$ spinels. *J. Solid State Chem.*, 2003, **176**(2), 549–555.
15. Tatsumi, K., Mizoguchi, T., Yoshioka, S., Yamamoto, T., Suga, T., Sekine, T. et al., Distribution of solute atoms in beta- and spinel $Si_{6-z}Al_zO_zN_{8-z}$ by Al K-edge X-ray absorption near-edge structure. *Phys. Rev. B*, 2005, **71**(3), art. no. 033202.
16. Jiang, J. Z., Kragh, F., Frost, D. J., Stahl, K. and Lindelov, H., Hardness and thermal stability of cubic silicon nitride. *J. Phys.: Condens. Matter*, 2001, **13**(22), L515–L520.
17. Jiang, J. Z., Lindelov, H., Gerward, L., Stahl, K., Recio, J. M., Mori-Sanchez, P. et al., Compressibility and thermal expansion of cubic silicon nitride. *Phys. Rev. B*, 2002, **65**(16), art. no. 161202.
18. Zerr, A., Kempf, M., Schwarz, M., Kroke, E., Göken, M. and Riedel, R., Elastic moduli and hardness of cubic silicon nitride. *J. Am. Ceram. Soc.*, 2002, **85**(1), 86–90.

19. Sekine, T. and Mitsuhashi, T., High-temperature metastability of cubic spinel Si_3N_4. *Appl. Phys. Lett.*, 2001, **79**(17), 2719–2721.
20. Paszkowicz, W., Minikayev, R., Piszora, P., Knapp, M., Baehtz, C., Recio, J. M. et al., Thermal expansion of spinel-type Si_3N_4. *Phys. Rev. B*, 2004, **69**(5), art. no. 052103.
21. Bruls, R. J., Hintzen, H. T., de With, G., Metselaar, R. and van Miltenburg, J. C., The temperature dependence of the Grueneisen parameters of $MgSiN_2$, AlN and beta-Si_3N_4. *J. Phys. Chem. Solids*, 2001, **62**(4), 783–792.
22. Krukowski, S., Leszczynski, M. and Porowski and S., *Properties, Processing and Applications of Gallium Nitride and Related Semiconductors*, INSPEC, Institution of Electrical Engineers, 1999, p. 2128.
23. Schwarz, M. R., *Synthesis of Novel Hard Materials: Spinel Si_3N_3 and Derivates*. PhD thesis, Technische Universität Darmstadt, Kassel University Press, 2003, ISBN: 3-89958-104-0.
24. Evans, D. L. and Fischer, G. R., Determination of the thermal expansion of Pt by X-ray diffraction. *AIP Conf. Proc.*, 1972 (3), 97–104.
25. Kirby, R. K., Platinum—a thermal expansion reference material. *Int. J. Thermophys.*, 1991, **12**(4), 679–685.
26. Schneider, J., Mirror heaters for high temperature X-ray diffraction. *Adv. X-ray Anal.*, 1993, **36**, 397–402.
27. Berar, J. F. and Lelann, P., ESDs and estimated probable-error obtained in Rietveld refinements with local correlations. *J. Appl. Cryst.*, 2002, **24**, 1–5.
28. Knapp, M., Baehtz, C., Ehrenberg, H. and Fuess, H., The synchrotron powder diffractometer at beamline B2 at HASYLAB/DESY: status and capabilities. *J. Synchrotron. Radiat.*, 2004, **11**, 328–334.
29. Schröder, R. H., Schmitz-Pranghe, N. and Kohlhaas, R., Experimentelle Bestimmung der Gitterkonstanten der Platinmetalle im Temperaturbereich von −190 bis 1709 °C. *Z. Metall.*, 1972, **63**(1), 12–16.
30. Roisnel, T. and Rodriguez-Carvajal, J., WINPLOR: a windows tool for powder diffraction pattern analysis. *Mater. Sci. Forum*, 2001, **378-381**(1), 118–123.
31. Yamai, I. and Ota, T., Thermal expansion of Sialon. *Adv. Ceram. Mater.*, 1987, **2**(4), 784–788.
32. Hintzen, H. T., Hendrix, M. R. M. M., Wondergem, H., Fang, C. M., Sekine, T. and de With, G., Thermal expansion of cubic Si_3N_4 with the spinel structure. *J. Alloy Compd.*, 2003, **351**(1/2), 40–42.
33. Berar, J. F. and Lelann, J., ESDS and estimated probable-error obtained in Rietveld refinements with local correlations. *J. Appl. Cryst.*, 1991, **24**(1), 1–5.